The Distribution of Mass in the Kuiper Belt

Matthew J. Holman[1]
Canadian Institute for Theoretical Astrophysics
McLennan Physical Labs
University of Toronto
60 St. George Street
Toronto, Ontario M5S 1A7
CANADA

ABSTRACT

The current understanding of the distribution of mass in the Kuiper belt is reviewed. A strategy for relating the orbital dynamics, overall mass, size distribution, and observations of Kuiper belt objects is outlined.

1. Introduction

Edgeworth (1949) and Kuiper (1951) first suggested that a collection of comets might be found in low-inclination, low-eccentricity orbits beyond Neptune. They pointed out that if the time scale for forming planets in this region is longer than the age of the solar system then remnant planetesimals might naturally be found there. These authors even noted that this region might provide a reservoir of short period comets. Fernandez (1980) suggested that massive comets in this belt would slowly scatter smaller planetesimals into Neptune- and Uranus-crossing orbits that would then evolve under planetary perturbations into visible short period comet orbits. However, it seems unlikely that comets massive enough to drive the flux of short period comets would go undetected in earlier observational surveys. Strong indirect evidence supporting the existence of such a comet belt came from Duncan *et al.* (1988) and Quinn *et al.* (1990). Beginning with a distribution of orbits with perihelia already in the outer planet region, these authors demonstrated through numerical integrations that the distribution of orbital elements of Jupiter-family short period comets is consistent with a flattened disk source, but that a spherical source such as the Oort Cloud would lead to a distribution of semimajor axis, inclination, and argument of perihelion that is not observed. They named this collection of comets the "Kuiper belt." The mechanism by which Kuiper belt comets develop Neptune-crossing orbits was identified independently by Holman and Wisdom (1993) and Levison and Duncan (1993). With numerical integrations of small bodies in the Kuiper belt they showed that the long-term gravitational perturbations of the outer planets can lead to large excursion in the eccentricities of belt objects. On time scales of

[1]Formerly at N.A.O., Mitaka, Tokyo, Japan

$10^8 - 10^9$ years some of the objects in the Kuiper belt undergo close encounters with Neptune. In contrast, other objects in the belt retain nearly circular orbits for times on the order of the age of the solar system. Obviously, the long-term dynamics affects the distribution of mass in the Kuiper belt. Where the time required to develop a Neptune-encountering orbit is short in comparison to the age of the solar system little material is likely to be found; where the time required is long primordial material would remain if that region were initially populated.

One of the primary goals of the investigations of the Kuiper belt is to estimate the overall mass and number of objects in the belt. A simple approach is to determine from numerical integrations the rate at which a population of objects in the belt is encountering Neptune and subsequently evolving into visible Jupiter-family comets. The size of the Kuiper belt population can then be determined by matching this rate to estimates for the observed rate of generation of new Jupiter-family comets. Holman and Wisdom (1993) exploited an empirical feature of the dynamics to estimate the current flux of Kuiper belt objects encountering Neptune from numerical integrations as short as 200 million years. They showed that the number of objects remaining in the Kuiper belt decreases as the logarithm of time. For example, roughly the same number of test particles encountered Neptune in $10^3 - 10^4$ years as in the interval $10^4 - 10^5$ years. This implies that the flux of objects is decaying slowly as $\sim 1/t$. This permits an extrapolation of the flux from 2×10^8 years to 4.5×10^9 years. Roughly 17% of the objects that encounter Neptune will subsequently evolve into visible short period comets (Duncan *et al.* 1988). The rate of generation of new short period comets was taken to be 0.01 year^{-1} (Fernandez 1985). From these values, Holman and Wisdom (1993) estimated that 9×10^9 objects were initially in the belt (30-50 AU) and that roughly half as many remain currently. Furthermore, it seems important to investigate the sensitivity of this result to changes in the initial population and to determine if it remains when longer integrations are completed.

The distribution of material in the Kuiper belt is constrained not only by the dynamics of individual objects in the belt but also by the collective effects of the mass in the belt on the dynamics of other solar system objects. In particular, a massive belt beyond Neptune would induce additional observable perihelion precession in some short period comets. By modeling the drift in the perihelion of P/Halley it is possible to show that the mass of the Kuiper belt cannot be larger than about $1M_\oplus$ (Hamid *et al.* 1968, Hogg *et al.* 1991) if the belt were concentrated at $\sim 40 - 50$ AU.

Although much insight has been gained from these theoretical investigations, the most direct constraint on the distribution of mass in the Kuiper belt comes from the observations. The first Kuiper belt object, 1992 QB1, was discovered in by Jewitt and Luu (1993). Reports of subsequent discoveries have been increasingly frequent. In the interest of brevity I refer the reader to the papers by Jewitt and Luu (1995) and Weissman (1995) for detailed summaries and discussions of the observational surveys that have been conducted to date. Here, I simply note that several teams of observers have discovered a total of 21 objects in ongoing observational surveys. These searches have been concentrated near the ecliptic and at times near the triangular Lagrange points of the outer planets. The limiting magnitudes of the successful surveys have been $R \approx 23 - 25$. Table 1 lists the orbital elements, R magnitude, geocentric distance near the time of discovery, as well as the estimated diameters of the currently known Kuiper belt objects. These data are based on the orbit solutions provided by Brian Marsden. The asterisks indicate those objects with tentative orbital solutions. Many of these objects have been observed at only one opposition, so their orbital elements are uncertain. The listed orbital elements are all consistent with the observations, however other solutions are possible and these solutions will be refined as future observations are available. Putting these concerns aside we can note several features of the data set. First, all of the semimajor axes lie in the range 39-48 AU. Many of the observations are consistent with resonant orbits. The objects with semimajor axes near 39.4 AU appear to be in the 3:2 mean-motion resonance with Neptune. This observation is supported by and motivates further dynamical investigations, such as the work of Malhotra (1993, 1995). These objects have high eccentricities, and many of them have large inclinations as well. These objects have orbits that are quite similar to that of Pluto, which is also in the 3:2 mean-motion resonance. As can be seen from the mean anomalies of these objects most have been discovered near perihelion. In part this may have been an assumption for estimating the orbital elements. In part this is to be expected, as the objects will be brightest at perihelion. The final column of the table lists the diameters of the objects in kilometers assuming a geometric albedo of 0.04 and neglecting phase angle effects. In the analysis of the results of a single observational survey of 1.2 sq. deg. which yielded seven discoveries Jewitt and Luu (1995) estimate that 35,000 objects with diameters greater than 100 km reside in the belt between 30 and 50 AU, assuming the inclinations are less than $i \sim 16°$. Jewitt and Luu (1995) and Weissman (1995) discuss the size distribution in detail. Given the observations, the primary question is: Can we find a model that self-consistently matches the observations and constraints which can be used to predict the distribution of orbital elements and sizes of Kuiper belt objects discovered in future, fainter observational surveys?

The next section presents two models for the dynamics of small bodies in the Kuiper belt. In Section 3 relations among the overall mass, the size distribution, the orbital dynamics, and the observations are used to constraint the distribution of mass in the belt. Section 4 outlines a method of developing predictions for the number of Kuiper belt objects that would be observed in fainter surveys, based on the models presented. Section 5 presents a list of possible avenues of future work.

2. Two Dynamical Models

There are two principal models for the dynamics of the Kuiper belt. The first model, developed by Holman and Wisdom (1993) and Levison and Duncan (1993), assumes that as the material beyond Neptune is gravitationally perturbed by the massive planets some of it develops planet-crossing orbits. This material is then either scattered into the inner solar system or is ejected from the solar system. It is assumed in this model that the planets have been following orbits similar to their present day orbits since their formation. In order to include the perturbations of the planets on the small bodies in the Kuiper belt the outer planets are integrated along with the test particles. The initial conditions of the planets are simply the current planetary positions and velocities. Given this model we would expect to find material in the Kuiper belt in the regions of phase space either where the estimated time required to develop planet crossing orbit is longer than the age of the solar system or where these objects are in stable orbits.

In the study of Holman and Wisdom (1993), a total of 1500 test particle orbits were integrated near and beyond Neptune. These were full n-body integrations including the gravitational perturbations of the Sun and four giant planets using the symplectic mapping method for the n-body problem (Wisdom and Holman, 1991). The duration of these integrations ranged from 1 billion years to 4.5 billion years. At intervals of 0.09 AU, groups of six test particles were started on circular orbits with different initial longitudes. Each test particle orbit was integrated until a close encounter with a planet occurred or until the maximum integration time was reached. Figure 1 shows the times of planetary close encounter for each of the test particles in the simulation. The line marks the minimum of the six times in each semimajor axis bin. The points mark the other times. From this figure the regions that are unstable on times much less than the age of solar system are quite clear. Likewise, the regions with longer time scales can be easily identified. It must be emphasized that the test particles represented by Figure 1 were all started on initially circular orbits in the invariable plane. Large initial eccentricities or inclinations would alter the results (see Levison and Duncan, 1993).

The second model relies on the idea that as the planets scattered smaller bodies during the stages of solar system formation the planets themselves wandered about due to exchange of orbital angular momentum with the planetesimals. The only numerical investigation of this process is due to Fernandez and Ip (1984). In some of their simulations Saturn, Uranus, and Neptune drift outward by a few AU while Jupiter drifts sunward by a few tenths of an AU. Malhotra (1993) proposed that this process is responsible for Pluto's resonant orbit. As Neptune evolved outward material beyond Neptune was swept by the mean-motion resonances with Neptune. Some of this material was be captured into these resonances. As Neptune continued to move outward the material trapped in resonance was naturally carried to high eccentricity. Pluto, with its highly eccentric resonant orbit, seems a likely candidate. In fact, this capture process is so efficient that it is expected that much of the material initially beyond Neptune would now be trapped in mean motion resonance with Neptune (Malhotra 1995).

Figure 2 represents the results of a simulation similar to that described in Malhotra (1993, 1995). This was accomplished by including an additional "drag" force in the equations of motion (see Malhotra 1995 for details). Here the time scale of the semimajor axis drift, τ, was 2 myr. The initial conditions of the planets were determined by integrating the system backwards 40 million years, so after 40 million years in the simulation the planets achieved their current orbital configuration. Jupiter, Saturn, Uranus, and Neptune drift by -0.2, 0.8, 3.0, and 7.0 AU, respectively. 300 test particles were placed in 22-52 AU at uniform intervals. The initial eccentricities were selected from a uniform distribution between 0.0 and 0.02. The inclinations were uniformly distributed between 0.0 and 0.02 radians. Figure 2 shows the histogram of the time averaged semimajor axes for those test particles that survived 792 million years. The time averaging began after the first 100 million years, enough time for the capture process to be completed. There are concentrations of test particles at the approximate locations of the 3:2, 5:3, and 2:1 mean motion resonances with Neptune at 39.4, 42.3, and 47.8 AU, respectively. Other regions hold much less material in a flatter distribution. Figure 3 and Figure 4 show the osculating semimajor axes of the surviving test particles after 792 million years versus eccentricity and inclination, respectively. Test particles have a much greater range of eccentricity at the locations of the mean-motion resonances, consistent with the capture process increasing the eccentricity as material is carried to larger semimajor axis. The inclinations also have a much greater range at the locations of the mean motion resonances, but the range is not consistent with the large inclination of Pluto. This was pointed out by Malhotra (1993, 1995), who explored the dependence of the range of inclination on the rate of drift of the planetary semimajor axes.

Both of the dynamical models describe how the distribution of mass in the Kuiper belt changes with time. In one model the distribution primarily is altered by removing material from regions where the eccentricities become large enough for planetary close encounters to occur. In the other models the distribution is altered by resonance capture. The next section outlines an approach for analyzing these effects.

3. Mass Distribution

The initial surface density in the inner Kuiper belt can be modeled as

$$\sigma_0(r) = \sigma_o(r_0)\left(\frac{r_0}{r}\right)^n, \tag{1}$$

where r is the heliocentric distance. Tremaine (1991) suggests $n = 2$ based on a fit to the non-volatile mass in the outer planets. Hayashi (1981) suggests $n = 3/2$, based on a minimum mass model of the solar nebula. A value of n =1 indicates that the mass contained in successive annuli is distributed uniformly as a function of heliocentric distance.

In order to estimate the *current* mass in the inner Kuiper belt based on the *initial* mass it is necessary to develop a model for the rate at which material is removed from the belt. A starting point is to assume that mass is removed primarily by close encounters with Neptune that either delivery the material to the inner solar system as a short period comets or eject it from the solar system. A simple approach is to assume that there exists an exponential time scale, $\tau(a)$, as a function of semimajor axis which governs the rate at which material is removed from the belt. The surface density as a function of time might then be written

$$\sigma_t(a) = \sigma_o(a)e^{-t/\tau(a)}. \tag{2}$$

The time scale could equally well be a function of all the orbital elements; there are obvious shortcomings to such a simple model. The exponential decay is intended only to be an approximation to the rate at which material is leaving the belt. With such a model much of the detail of the dynamics of individual test particles is ignored in order to get some parameterization of the overall behavior.

Given equation (2), the overall mass in the inner Kuiper belt is given by

$$M_{kb} = \int_{a_{inner}}^{a_{outer}} 2\pi a \sigma_0(a) e^{-t/\tau(a)} da \tag{3}$$

Assuming the flux of new short period comets is composed primarily of Kuiper belt objects that have encountered Neptune, the flux will be proportional to the rate of change of mass in the inner Kuiper belt:

$$f_{spc} \propto -\frac{dM(t)}{dt} = \int_{a_{inner}}^{a_{outer}} 2\pi a \sigma_0(a) \frac{1}{\tau(a)} e^{-t/\tau(a)} da \tag{4}$$

The time scale as a function of semimajor axis can be estimated from the results of numerical investigations. This is straightforward for the study of test particle dynamics in the outer solar system by Holman and Wisdom (1993). In each semimajor axis bin, the times of close encounter along with the number of test particles that survived the full integration without a close encounter can be combined to estimate the removal time scale. Note that we simply use the initial semimajor axis for each test particle rather than an averaged value. This assumes that the semimajor axes of Kuiper belt objects remain roughly fixed, an assumption that is supported by the results of the numerical integrations. Typically, the semimajor axis of a test particle oscillates about a mean value and only changes dramatically after the eccentricity is large enough to permit close encounters with Neptune.

We estimate the time scales and associated errors following the treatment of Bartlett (1953). Starting with N test particles, the qth particle is integrated for a time T_q. The probability that n particles have close encounters in the course of the integrations and that $N - n$ particles remain at the end of the integrations is given by

$$P = \binom{N}{n} \prod_{r=1}^{n} \left(e^{-t_r/\tau} \frac{dt_r}{\tau} \right) \prod_{s=n+1}^{N} e^{-T_s/\tau}. \tag{5}$$

Given that at least one close encounter occurred during the integration ($n \geq 1$), the value of τ that maximizes this probability is:

$$\hat{\tau} = \frac{1}{n} \left[\sum_{r=1}^{n} t_r + \sum_{s=n+1}^{N} T_s \right]. \tag{6}$$

The Bartlett S-function is used to estimate the error associated with $\hat{\tau}$. For this problem, the S-function is:

$$S(\tau) = \frac{n \left(\frac{\hat{\tau}}{\tau} - 1 \right)}{\sqrt{\sum_{q=1}^{N} \left(1 - e^{-T_q/\tau}\right)}} \tag{7}$$

The error bounds for τ are given by $S(\tau_-) = 1$ and $S(\tau_+) = -1$. This technique is well suited to estimating decay time scales from a small number of samples that may be observed for different lengths of time. Given that the sample size is limited to six test particles in each semimajor axis bin, the associated errors are quite large. Typically $\tau_- \sim 0.5\hat{\tau}$ and $\tau_+ \sim 2.0\hat{\tau}$.

In the cases where none of the test particles in a given semimajor axis bin encountered a planet before the end of the integrations, the estimate of the decay time scale is not straightforward. Although the possible values are constrained by the fact that all of the particles remain at the end the integration, we simply assume in such a case that all of the material remains indefinitely, i.e. the time scale is infinite.

Figure 5 shows the decay time scale as a function of semimajor axis throughout the outer planet region. The ranges of semimajor axis surrounding each of the planets have been excluded as an exponential decay model is not even crudely correct in those regions. Likewise, the semimajor axis bins in which all of the test particles remain at the end of the integration have been excluded.

To test that the exponential decay model adequately represents the overall dynamics in the Kuiper belt, we compare the empirically computed number of test particles remaining beyond Neptune as a function of time to a simulation based on selecting six samples from an exponential distribution at each semimajor axis bin using the estimated decay time scales. Figure 6 shows this comparison. Although there are some differences, the overall profile of the two curves is the same. Other simple models can be used to fit the distribution of decays times for different collections of particles with reasonable success. The distributions simply parameterize the data in a way that is useful for analysis.

In order to relate the mass in the belt to the flux of new short period comets it is necessary to model the size distribution of Kuiper belt objects. Given that little is known about the physical characteristics of the current collection of Kuiper belt objects other than absolute magnitudes, a simple model for the size distribution will be used. Following Tremaine (1991) we assume that the number of objects with radii between R and $R + dR$ is given by $n(R)dR$, where

$$n(R) = \begin{cases} \frac{K}{R_0}\left(\frac{R_0}{R}\right)^{b_1+1} & \text{if } R < R_0 \\ \frac{K}{R_0}\left(\frac{R_0}{R}\right)^{b_2+1} & \text{if } R > R_0 \end{cases} \tag{8}$$

Tremaine (1991) suggests $b_1 = 2$ is consistent with the size distribution of comets, as well as the cratering record on the outer planet satellites. A value of $R_0 = 10\ km$ is selected and a range of values of b_2 can be explored. The results described below can be developed for a variety of size distributions. Only one is developed as an example. The total mass predicted by this distribution is

$$M = \int_0^\infty \frac{4\pi}{3}\rho R^3 n(R) dR = \frac{4\pi}{3}\rho R_0^3 K C, \tag{9}$$

where $C = \frac{1}{3-b_1} + \frac{1}{b_2-3}$. Likewise, the number of objects larger than a given size, R_{min}, is related to the total mass by

$$N_{>R_{min}} = \begin{cases} \frac{K}{b_1}\left[\left(\frac{R_0}{R_{min}}\right)^{b_1} - 1\right] + \frac{K}{b_2} & \text{if } R_{min} < R_0 \\ \frac{K}{b_2}\left(\frac{R_0}{R_{min}}\right)^{b_2} & \text{if } R_{min} > R_0 \end{cases} \tag{10}$$

By combining the equations we have

$$f_{spc} = C_{spc}\frac{1}{\frac{4\pi}{3}\rho {R_0}^3 C}\left(\frac{1}{b_1}\left[\left(\frac{R_0}{R_{min}}\right)^{b_1} - 1\right] + \frac{1}{b_2}\right)\int_{r_{inner}}^{r_{outer}} 2\pi r \sigma_0(r)\frac{1}{\tau(r)}e^{-t/\tau(r)}dr, \tag{11}$$

where C_{spc} represents the fractions of those objects encountering Neptune which become visible short period comets. It is assumed that $R_{min} < R_0$ as R_0 was chosen to be roughly the largest comet radius. It is clear that f_{spc} is only weakly dependent on the value of b_2 except in determining the value of C. Therefore, we have

$$f_{spc}(t) \approx C_{spc}\frac{1}{\frac{4\pi}{3}\rho {R_0}^3 C b_1}\left(\frac{R_0}{R_{min}}\right)^{b_1}\int_{r_{inner}}^{r_{outer}} 2\pi r \sigma_0(r_0)\left(\frac{r_0}{r}\right)^n \frac{1}{\tau(r)}e^{-t/\tau(r)}dr. \tag{12}$$

The value of $\sigma_0(r_0)$ governs the overall mass distribution. For $n = 1$, $n = 3/2$, and $n = 2$, respectively, we have

$$\sigma_0(r_0) \approx \left\{\begin{array}{l} 1.8 \times 10^{-4}\frac{M_\oplus}{AU^2}\left(\frac{10AU}{r_0}\right)^1 \\ 3.5 \times 10^{-4}\frac{M_\oplus}{AU^2}\left(\frac{10AU}{r_0}\right)^{1.5} \\ 6.8 \times 10^{-4}\frac{M_\oplus}{AU^2}\left(\frac{10AU}{r_0}\right)^2 \end{array}\right\} h\left(\frac{f_{spc}}{10^{-2}yr^{-1}}\right)\left(\frac{0.2}{C_{spc}}\right)\left(\frac{C}{3}\right)\left(\frac{b_1}{2}\right)\left(\frac{R_{min}}{1km}\right)^{b_1}, \tag{13}$$

where $h = \left(\frac{\rho}{1g/cm^3}\right)\left(\frac{R_0}{10km}\right)^{3-b_1}$. Note that the results are insensitive to the boundaries specified for the inner Kuiper belt as long as the limits encompass the regions from which objects develop Neptune-encountering objects at the time, t. In other regions, either the factor $\frac{1}{\tau(r)}$ or the factor $e^{-t/\tau(r)}$ is approximately zero. We choose $r_{inner} = 30$ AU and $r_{outer} = 50$ AU.

Studies of test particle stability in the outer solar system indicate that beyond about 43 AU all test particles started with small eccentricities and inclinations maintain that type of orbit for times comparable to the age of the solar system. Based on this result, we simply assume that surface density can be extrapolated assuming no mass has been removed by close encounters with Neptune beyond 43 AU. Given the estimates of $\sigma_0(r_0)$ it is possible to extend the model of the inner Kuiper belt to greater distances. We give two sets of estimates for the mass of the inner Kuiper belt. The first includes the mass inside of 50 AU. The second includes the mass extrapolated to 100 AU. Each set gives the mass for $n = 1$, $n = 3/2$, and $n = 2$, respectively.

$$M_{<50AU} \approx \left\{ \begin{array}{l} 1.1\times 10^{-1} M_\oplus \left(\frac{\sigma_0(r_0)}{1.8\times 10^{-4}\frac{M_\oplus}{AU^2}}\right)\left(\frac{r_0}{10AU}\right)^{1} \\ 1.0\times 10^{-1} M_\oplus \left(\frac{\sigma_0(r_0)}{3.5\times 10^{-4}\frac{M_\oplus}{AU^2}}\right)\left(\frac{r_0}{10AU}\right)^{1.5} \\ 9.5\times 10^{-2} M_\oplus \left(\frac{\sigma_0(r_0)}{6.8\times 10^{-4}\frac{M_\oplus}{AU^2}}\right)\left(\frac{r_0}{10AU}\right)^{2} \end{array} \right\} \tag{14}$$

$$M_{<100AU} \approx \left\{ \begin{array}{l} 6.8\times 10^{-1} M_\oplus \left(\frac{\sigma_0(r_0)}{1.8\times 10^{-4}\frac{M_\oplus}{AU^2}}\right)\left(\frac{r_0}{10AU}\right)^{1} \\ 5.1\times 10^{-1} M_\oplus \left(\frac{\sigma_0(r_0)}{3.5\times 10^{-4}\frac{M_\oplus}{AU^2}}\right)\left(\frac{r_0}{10AU}\right)^{1.5} \\ 3.9\times 10^{-1} M_\oplus \left(\frac{\sigma_0(r_0)}{6.8\times 10^{-4}\frac{M_\oplus}{AU^2}}\right)\left(\frac{r_0}{10AU}\right)^{2} \end{array} \right\} \tag{15}$$

Of course, these formulas inherit all the dependences on parameters of $\sigma_0(r_0)$.

This kind of analysis cannot yet to be applied to the scenario of Malhotra (1993, 1995). Estimating the time scales for the model proposed by Malhotra (1993, 1995) requires more attention. In this case there are two stages that affect the distribution of mass. First, as Neptune drifts outward much of the material that is not captured into mean-motion resonance quickly encounters Neptune. The material that is captured is pushed to high semimajors axes along with Neptune. Second, after the Neptune has completed its outward drift the long-term perturbations of the planets can force some of the remaining material to encounter Neptune, as in the first model. Here, associating a decay time scale with specific collections of test particles is more difficult. The stability of an individual particle is a strong function of all of the orbital elements, not just the semimajor axis. Although it is interesting that many of the objects are captured into mean-motion resonances with Neptune, it remains to be seen if this scenario will provide a flux of short period comets. This work is in progress.

4. Observations

Given that the mass and size distributions in the Kuiper belt the next step is to estimate the number of objects that are observable with a given limiting magnitude. For a mass M at a heliocentric distance r, the approximate number of objects brighter than magnitude V is

$$N = \frac{M}{\frac{4\pi}{3}\rho {R_0}^3 C b_2} {R_0}^{b_2} \left(A^{-1/2} \frac{r^2}{r_\oplus} 10^{-0.2(V-V_\odot)} \right)^{-b_2}, \tag{16}$$

assuming that the smallest visible object is larger than R_0 and ignoring phase angle effects (Tremaine 1991). This follows from the size distribution and the relation between the size and magnitude:

$$V - V_{\odot} = -2.5 \log \left(\frac{\phi(\alpha) A R^2 r_{\oplus}^2}{r^2 \Delta^2} \right), \tag{17}$$

where A is the geometric albedo, $\phi(\alpha) \approx 1$ is the phase function, $V_{\odot}$ is the magnitude of the sun viewed from Earth with a specified filter, V is the magnitude of the object with the same filter, r is the heliocentric distance of the object, Δ is the geocentric distance of the object, and $r_{\oplus}$ is the heliocentric distance of the Earth. Note that

$$H = V - 5 \log(\frac{r\Delta}{r_{\oplus}^2}) \tag{18}$$

is the absolute magnitude. For example, the absolute magnitude of 1992 QB1 through a Johnson R filter is $H_R = 6.6$, and the magnitude of the sun through the same filter is -27.26 (Allen). Following Jewitt and Luu (1992), we assume $A = 0.04$, this implies $R \approx 125km$. Equation 16 can be easily combined with the distribution of mass in the inner Kuiper belt,

$$N = \int_{r_{min}}^{r_{max}} \frac{2\pi r \sigma(r)}{\frac{4\pi}{3} \rho {R_0}^3 C b_2} {R_0}^{b_2} \left(A^{-1/2} \frac{r^2}{r_{\oplus}} 10^{-0.2(V - V_{\odot})} \right)^{-b_2} dr \tag{19}$$

Figure 7 shows the cumulative number of Kuiper belt objects visible to a specific semimajor axis. This is shown for three limiting magnitudes. These results assume $b_1 = 2.0$, $b_2 = 3.5$, and $n = 2$. The total mass in the belt for this model comes from equation 14. Please note that the results are highly dependent upon the size distribution, which is uncertain. Constraining the size distribution based on the observations will be left to future work.

5. Discussion

This paper outlined an approach for combining the results of numerical investigations into the long-term dynamics of small bodies in the Kuiper belt with actual observations of these objects. There are several avenues for future work.

1. The results of the simulations of the mechanism proposed by Malhotra need to be compared to the observations. In these cases the high eccentricities of the orbits can lead to a strong selection effect as these objects would be significantly brighter at perihelion. In this case, more detailed calculations need to be done to estimate the number of Kuiper belt objects that would be visible for various limiting magnitudes.

2. Again, for the scenario proposed by Malhotra longer numerical integrations are necessary to check if enough Kuiper belt objects would encounter Neptune to supply the observed

flux of short period comets. A lack of flux would require a re-thinking of the models and parameters. Figure 8 shows the number of test particles remaining in the simulation as a function of time. As in the model with non-drifting planets, the decay is quite slow. It remains to be checked if this decay rate is consistent with the current flux of short-period comets for reasonable Kuiper belt masses.

3. The size distribution of the Kuiper belt objects is uncertain. Jewitt and Luu (1995) examined this with Monte Carlo simulations that did not include a distribution of mass based on dynamical models. Combining this type of simulation with the results of dynamical investigations would yield a more complete answer.

4. One possible way to test between the two scenarios or to suggest a different scenario for the origin of the orbit of Pluto is to examine the distribution of orbital elements of Kuiper belt objects. In the scenario of Levison and Stern (1995) the origin of Pluto's orbit is due to the combined effects of gravitational perturbations at resonance and the effects of physical collisions and close encounters with planetesimals. The efficiency of this process depends strongly on the collisional cross section of Pluto and the density of other objects in the vicinity. One might expect in this case that only the largest objects would be trapped in resonance. Malhotra's capture mechanism, in contrast, would be equally efficient for a wide range of sizes. In this case we would expect to find a large number of objects trapped in orbits similar to Pluto's. There appears to be evidence for this in the observations.

6. Acknowledgements

I would like to thank Brian Marsden for supplying me with orbital elements of the current Kuiper belt objects. I also thank Haruo Yoshida, Hiroshi Kinoshita, Jun-ichi Watanabe, Scott Tremaine, Jack Wisdom, Norm Murray, and Jihad Touma for helpful conversations. I am grateful for the hospitality of the people at the National Astronomical Observatory of Japan, in Mitaka, where much of this work was carried out. This work was supported in part by a post-doctoral fellowship from the Japan Society for the Promotion of Science.

7. References

Allen. (1971). *Astrophysical Quantities*, 3rd ed. Athlone Press, London.

Bartlett, M. S. (1953). On the statistical estimation of mean life-times. *Philosophical Magazine* **44**, 249.

Duncan, M., Quinn, T., and Tremaine, S. (1988). *Ap. J.* **328**, L69.

Edgeworth, K. E. (1949). The origin and evolution of the solar system. *MNRAS* **109**, 600-609.

Fernandez, J. A. (1980). *MNRAS* **192**, 481.

Fernandez, J. A. (1985). *Icarus* **64**, 308.

Fernandez, J. A., and Ip, W.-H. (1984). Some dynamical aspects of the accretion of Uranus and Neptune: the exchange of orbital angular momentum with planetesimals. *Icarus* **58**, 109-120.

Hamid, S. E., Marsden, B. G., and Whipple, F. L. (1968). *Astron. J.* **73**, 727.

Hogg, D. W., Quinlan, G. D., and Tremaine, S. (1991). Dynamical limits on dark mass in the outer solar system. *Astron. J.* **101**, 2274-2286.

Holman, M. J. and Wisdom, J. (1993). Dynamical stability in the outer solar system and the delivery of short period comets. *Astron. J.* **105**, 1987-1999.

Jewitt, D. and Luu, J. X. (1993). Discovery of the candidate Kuiper belt object 1992 QB1. *Nature* **362**, 730-732.

Jewitt, D. C., and Luu, J. X. (1995). The solar system beyond Neptune. submitted to *Astron. J.*

Kuiper, G. P. (1951). On the origin of the solar system. In *Astrophysics*, ed. Hynek. 357-424.

Levison, H. and Duncan, M. (1993). *Astrop. J.* The gravitational sculpting of the Kuiper belt. **406**, L35-L38.

Levison, H. F. and Stern, S. A. (1995). Possible Origin and Early Dynamical Evolution of the Pluto-Charon Binary. Submitted to *Icarus*.

Malhotra, R. (1995). The origin of Pluto's orbit: implications for the Solar System beyond Neptune. preprint.

Malhotra, R. (1993). The origin of Pluto's peculiar orbit. *Nature* **365**, 819-821.

Quinn, T., Tremaine, S., and Duncan, M. (1990). *Ap. J.* Planetary perturbations and the origin of short-period comets. **355**, 667-679.

Stern, S. A. (1991). *Icarus* On the number of planets in the solar system: evidence of a population of 1000-km bodies. **90**, 271-281.

Tremaine, S. (1990). In *Baryonic Dark Matter*, ed. D. Lyndon-Bell and G. Gilmore, 37-65.

Watanabe, J. (1994). Kuiper belt survey by Subaru Telescope. *Proceedings of Subaru Telescope Conf.* in press.

Weissman, P. R. (1995). The Kuiper belt. preprint.

Yamamoto, T., Mizutani, H., and Kadota, A. (1994). Are 1992QB1 and 1993FW Remnant Planetesimals?. *PASJ.* **46**, L5-L9.

object	a	e	i	Ω	ω	M	m_r	r	H	D
1992QB1	43.94	0.07	2.2	359.4	357.3	5.8	22.7	39.9	6.6	250
1993FW	43.82	0.05	7.7	187.9	35.2	329.8	22.8	41.1	6.6	250
1993RO	39.34	0.20	3.7	170.3	187.4	357.1	22.9	30.5	8.0	130
1993RP*	39.33	0.11	2.6	192.1	180.6	360.0	24.4	33.9	9.0	80
1993SB	39.39	0.32	1.9	354.8	79.1	319.7	23.0	31.2	8.0	130
1993SC	39.47	0.18	5.2	354.6	319.2	33.9	21.7	33.1	6.4	280
1994ES2	45.93	0.12	1.0	154.7	99.6	279.2	24.1	44.7	7.5	170
1994EV3	43.07	0.04	1.7	19.5	13.1	166.1	23.5	43.7	7.0	210
1994GV9	43.39	0.04	0.50	176.9	317.0	37.8	23.2	41.0	7.0	210
1994JS*	39.40	0.08	14.6	0.3	180.0	360.0	22.3	35.2	6.8	230
1994JV*	39.46	0.12	16.8	0.2	180.0	360.0	22.3	33.5	7.0	210
1994JQ1	44.31	0.03	3.7	25.6	197.4	348.1	23.3	42.1	7.0	210
1994JR1	39.76	0.13	3.80	144.7	116.8	347.5	22.8	33.8	7.5	170
1994TB*	39.53	0.28	12.4	0.2	82.3	117.0	22.3	29.8	7.5	170
1994TG*	42.25	0.00	6.80	15.5	353.0	0.0	23.2	41.3	7.0	210
1994TH*	40.94	0.00	16.1	0.1	356.6	0.0	23.1	39.9	7.0	210
1994TG2*	42.45	0.00	2.20	353.3	358.9	359.9	23.2	41.4	7.0	210
1994VK8*	43.45	0.00	1.40	72.8	349.0	0.0	22.2	42.5	5.9	350
1995DA*	47.57	0.30	5.40	127.4	0.4	0.0	23.1	32.1	8.0	130
1995DB2*	47.62	0.15	3.20	128.6	0.2	0.0	23.0	39.3	7.0	210
1995DC2*	45.41	0.00	0.90	156.0	357.0	0.0	23.0	44.4	6.5	260

Table 1: For the epoch of 24.0 March 1995 the elements of the current Kuiper belt objects are listed in order of discovery. Ecliptic and equinox of J2000.0. Semimajor axis in AU, eccentricity, inclination, longitude of the ascending node, argument of perihelion, and mean anomaly (degrees). Following is the R magnitude and the geocentric distance (AU) at the epoch, as well as the diameter (km).

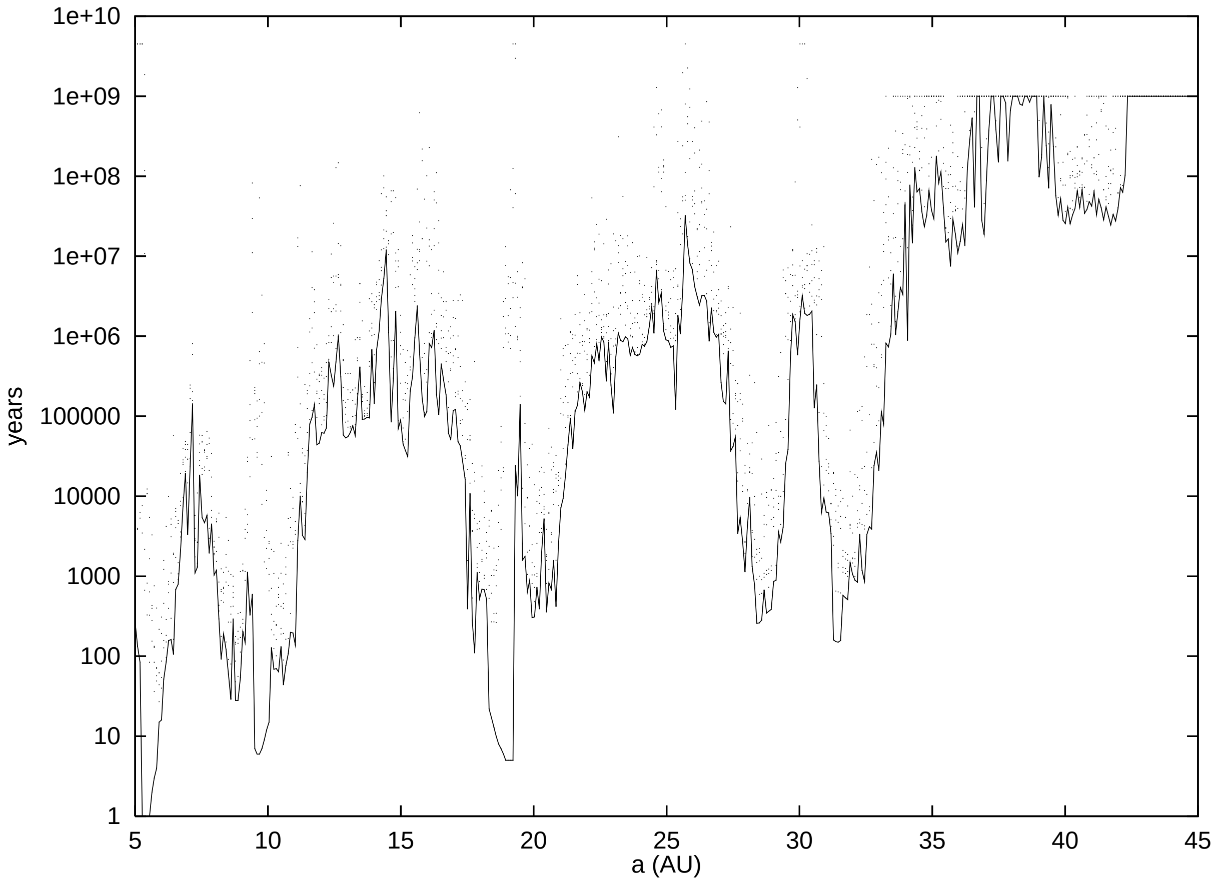

Fig. 1.— The time survived by each test particle is plotted as a function of initial semimajor axis. For each semimajor axis bin, six test particles were started at different longitudes. The points mark the termination times of the six test particles. The line below the points marks the envelope of the minimum termination times. The scatter of points gives an idea of the spread of termination times for any given semimajor axis. The envelope at the top is the mark of those test particles surviving the full integration. The spikes at 5.2, 9.5, 19.2, and 30.1 AU, at the semimajor axes of the planets, correspond to test particles librating in Trojan or horseshoe-like orbits before close encounter. Interior to Neptune the integration extends to 800 million yr; exterior to Neptune the integration reaches 200 million yr. Beyond about 43 AU all the test particles survive the full integration.

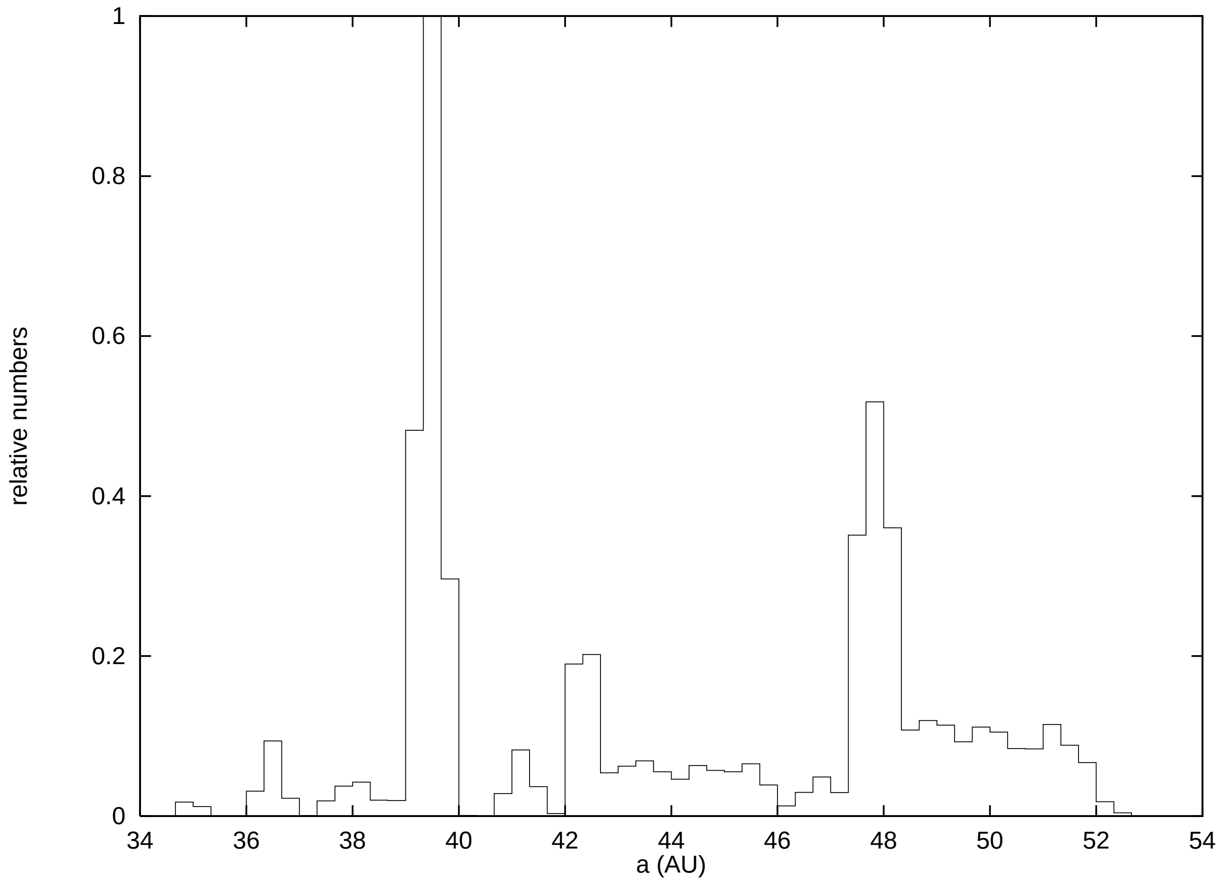

Fig. 2.— The figure shows the time averaged histogram of semimajor axes for those test particles that have not encountered Neptune as of 792 million years. The time averaging began after the first 100 million years, enough time for the capture process to be completed. There are concentrations of test particles at the approximate locations of the 3:2, 5:3, and 2:1 mean motion resonances with Neptune at 39.4, 42.3, and 47.8 AU, respectively. Smaller concentrations can be identified at other resonance locations. Other regions hold much less material in a flatter distribution.

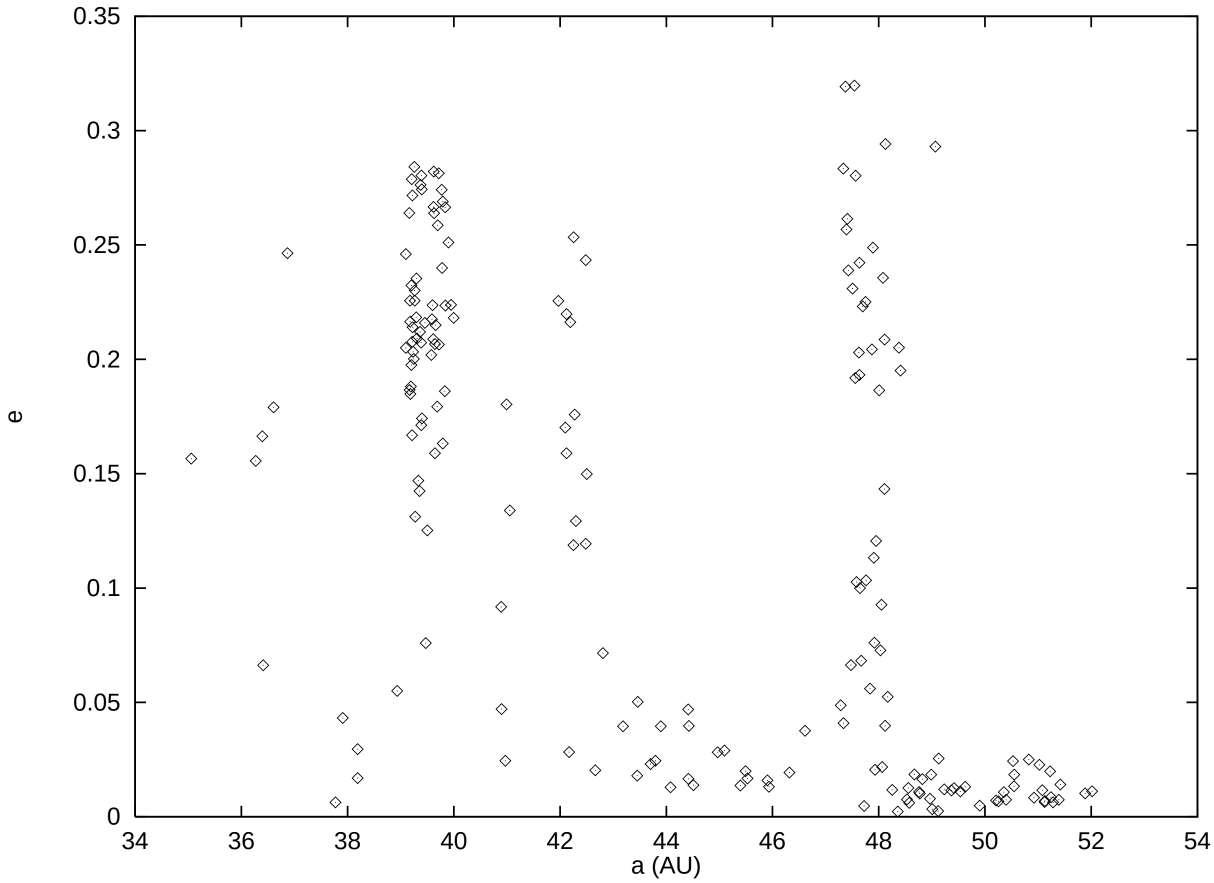

Fig. 3.— The osculating semimajor axes of the surviving test particles after 792 million years are plotted versus the eccentricity. Test particles have a much greater range of eccentricity at the locations of the mean-motion resonances, consistent with the capture process increasing the eccentricity as material is carried to larger semimajor axis.

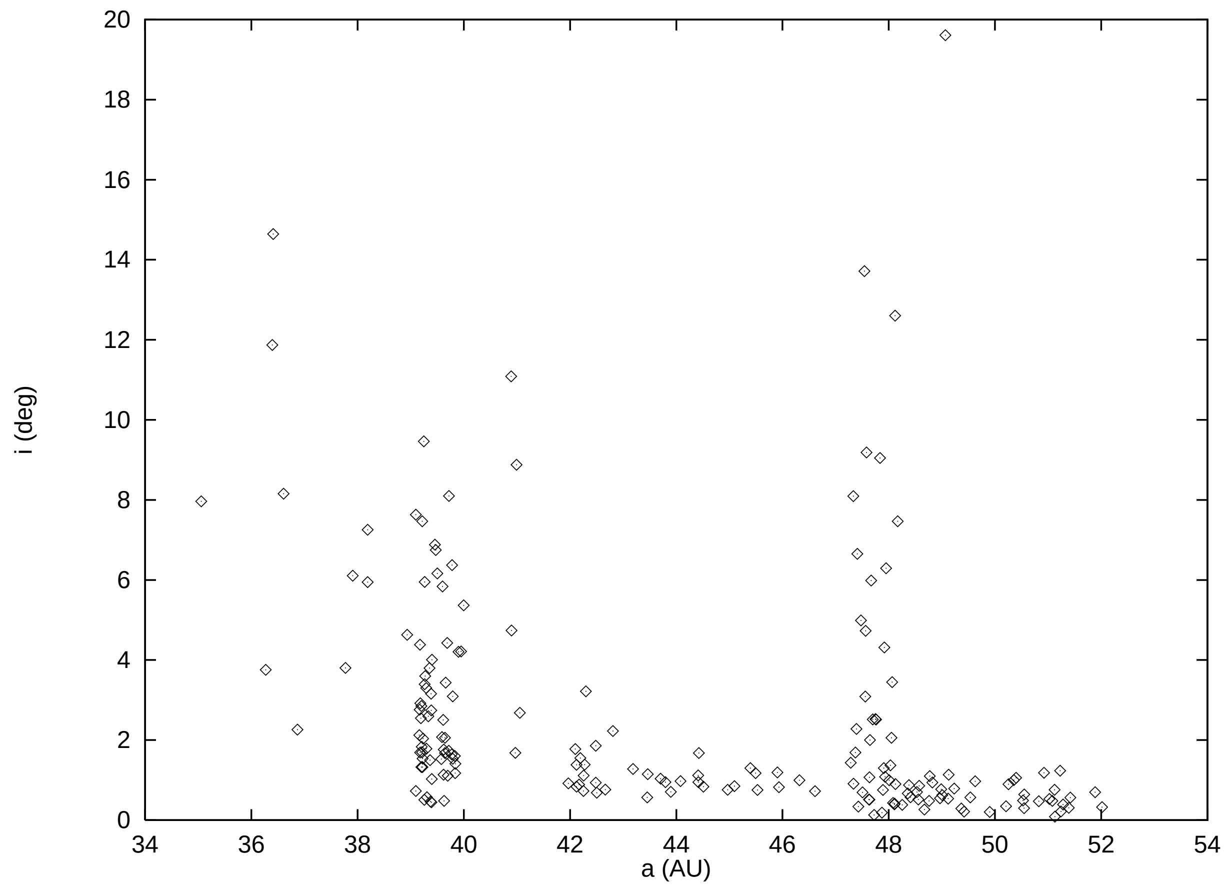

Fig. 4.— The osculating semimajor axes of the surviving test particles after 792 million years are plotted versus the inclination. Test particles have a much greater range of inclination at the locations of the mean-motion resonances. The range of inclination is not consistent with the larger inclination (17°) of Pluto. This may be a function of the rate of drift of the planetary semimajor axes.

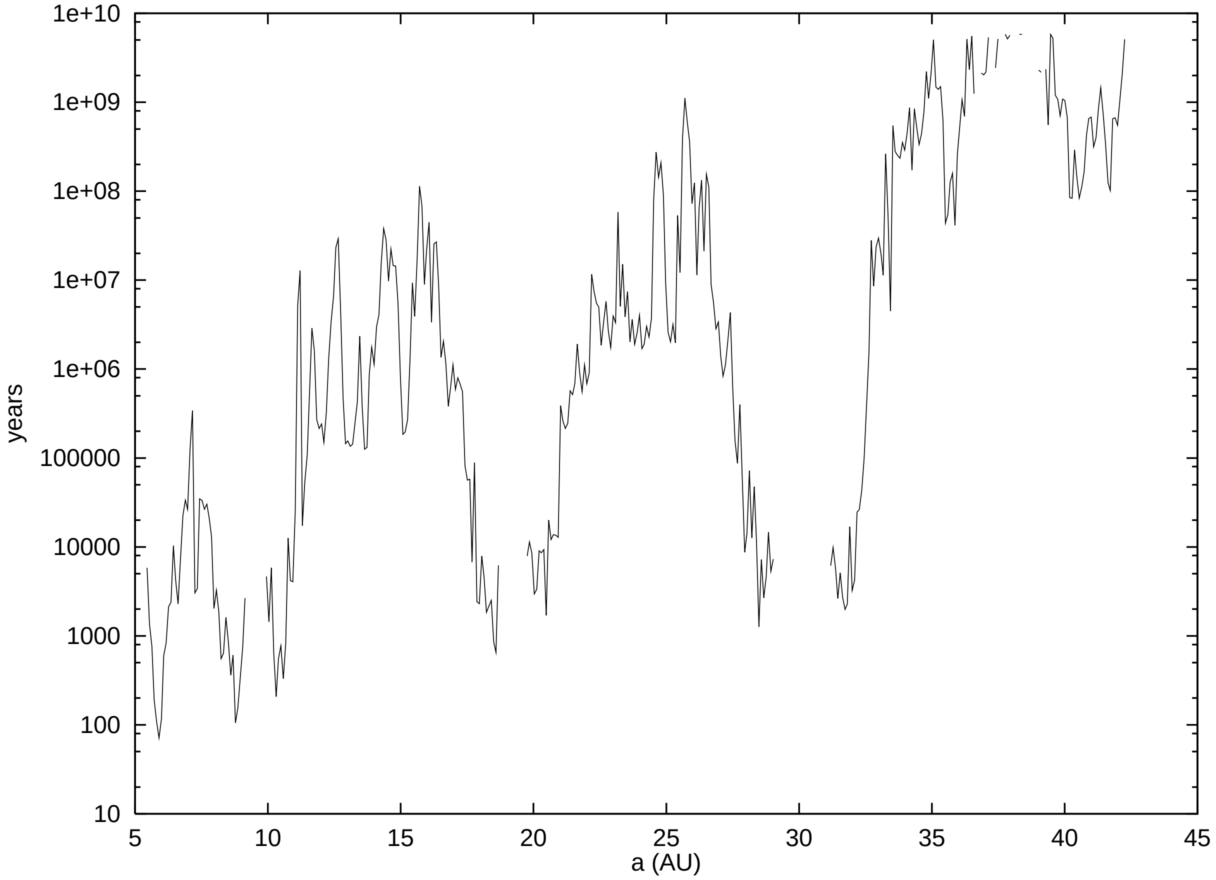

Fig. 5.— The estimated decay timescale is plotted as a function of initial semimajor axis.

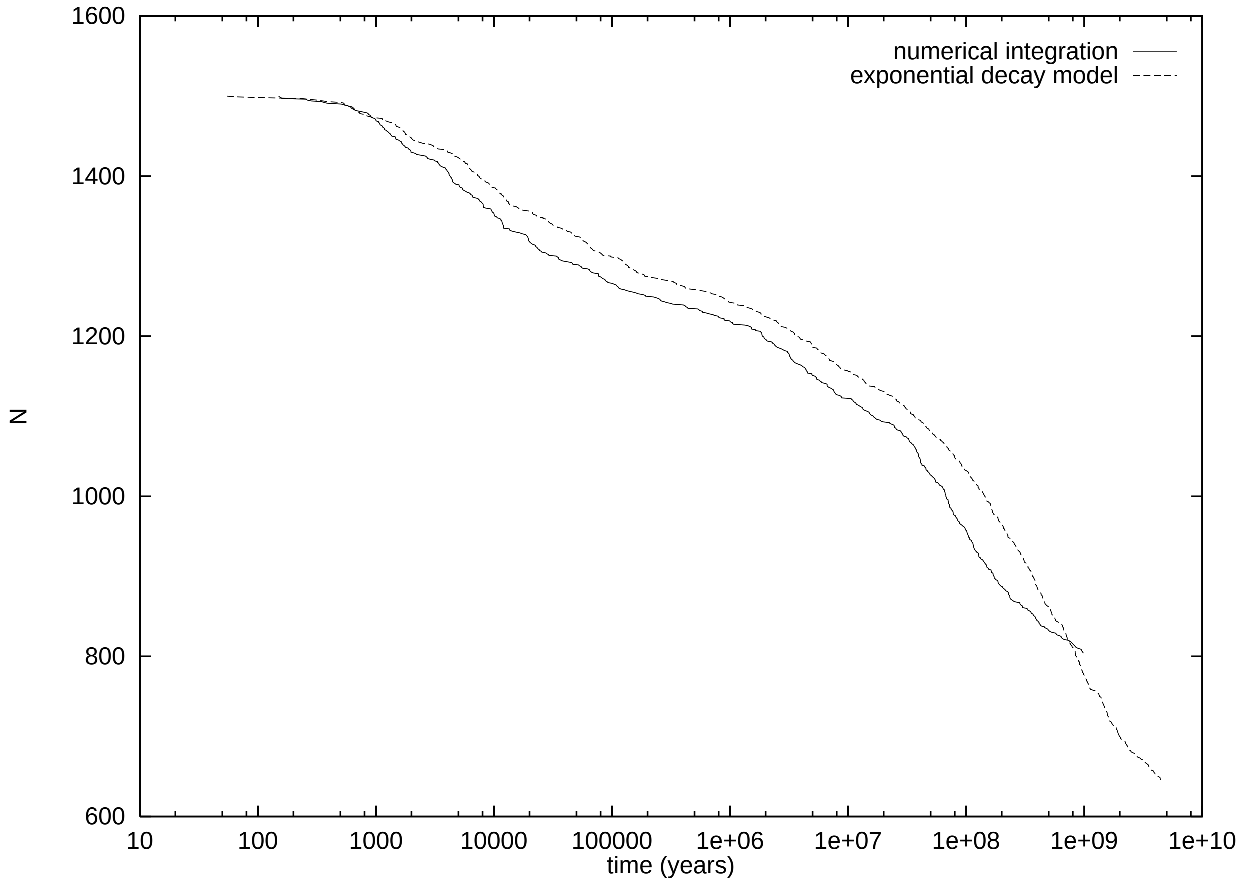

Fig. 6.— The number of test particles remaining beyond Neptune is plotted versus the logarithm of time. One line shows the results from the numerical integrations. The other line shows the results of a simulation of the decay process, assuming the exponential time scales shown in the previous figure.

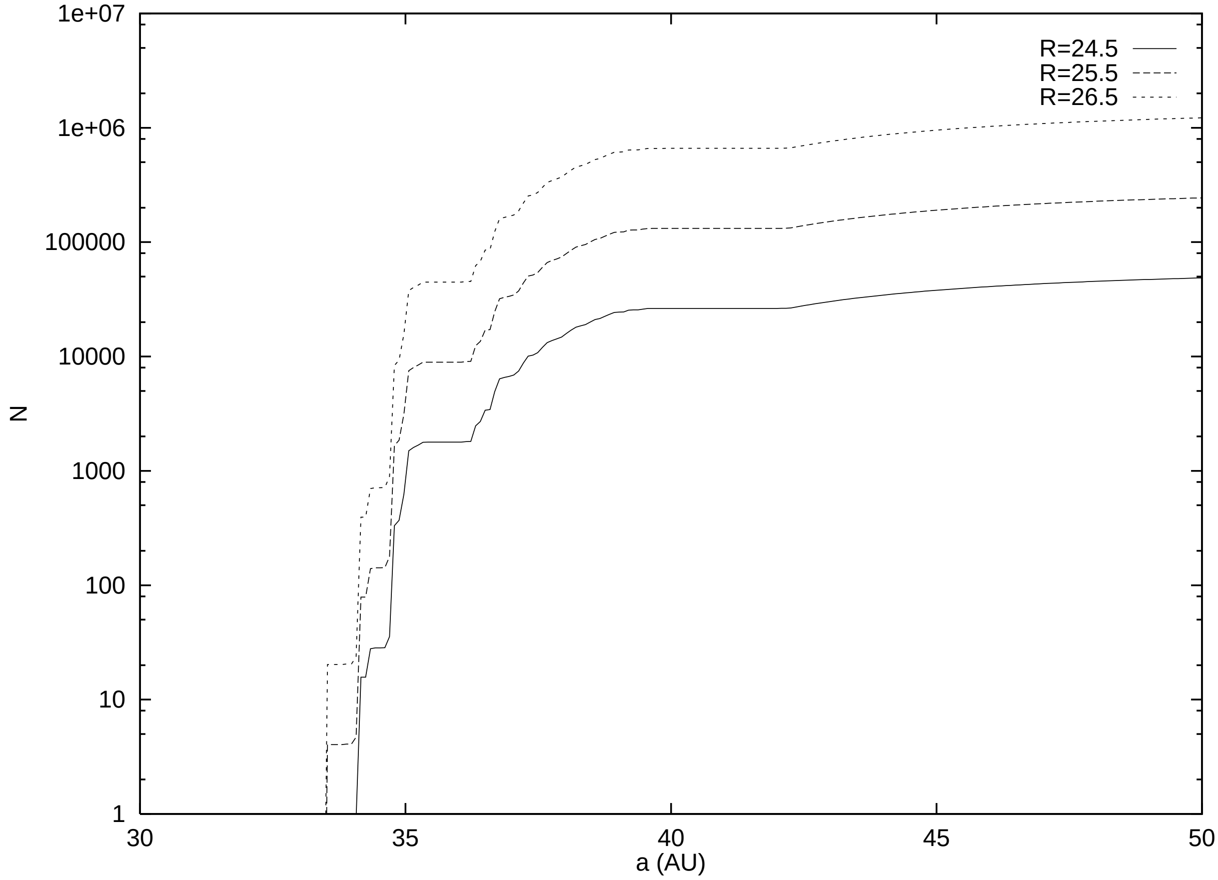

Fig. 7.— This figure shows the estimated number of visible Kuiper belt objects as a function of semimajor axis and limiting magnitude.

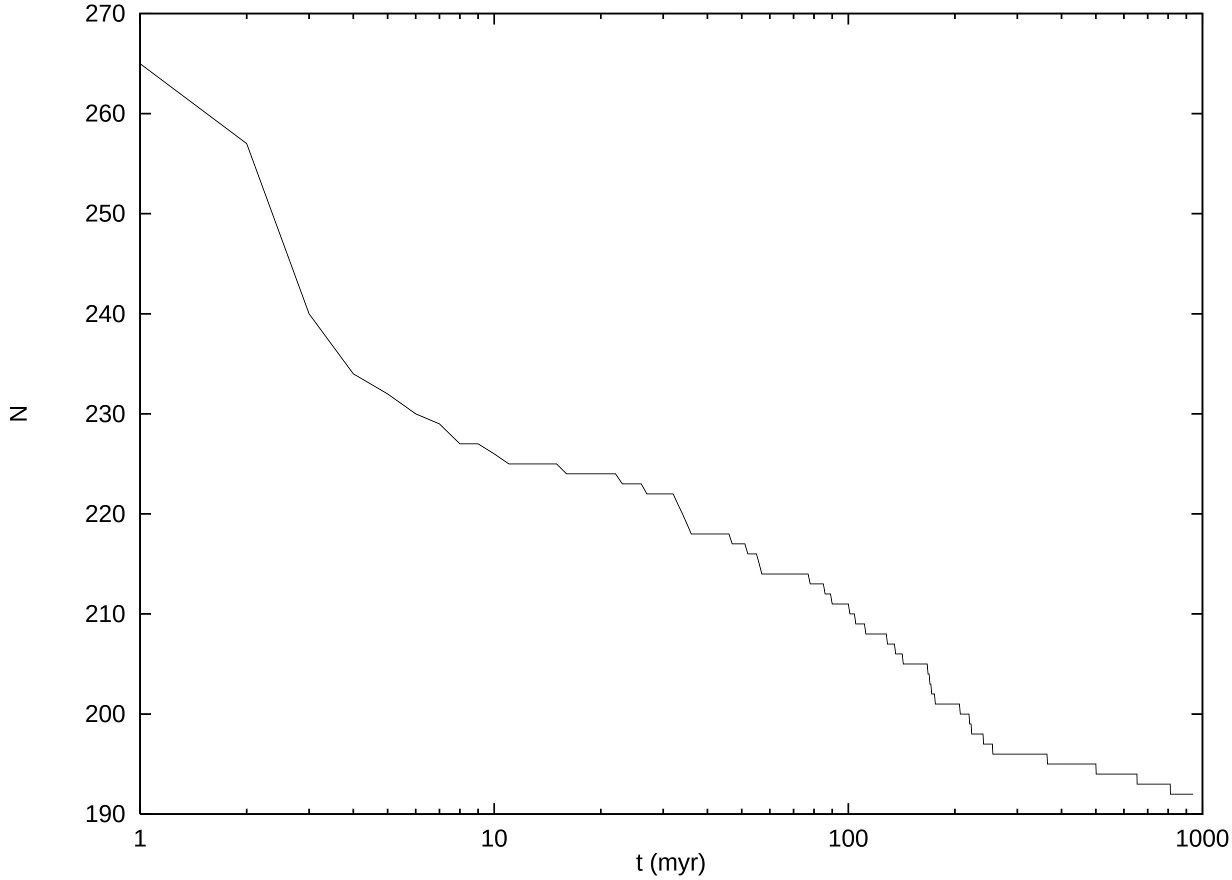

Fig. 8.— This figure shows the number of test particles remaining beyond Neptune as a function of time. The first 20 myr is marked by a rapid decrease in the population due to the outward drift of Neptune.